



## Functionalization of boron-doped tri(9,10-anthrylene)s



Claas Hoffend, Kai Schickedanz, Michael Bolte, Hans-Wolfram Lerner, Matthias Wagner\*

Institut für Anorganische Chemie, J.W. Goethe-Universität Frankfurt, Max-von-Laue-Strasse 7, D-60438 Frankfurt (Main), Germany

### ARTICLE INFO

#### Article history:

Received 3 May 2013

Received in revised form 5 June 2013

Accepted 11 June 2013

Available online 18 June 2013

#### Keywords:

Organoboranes

Charge transfer

Electrochemistry

Halogenation reactions

Fluorescence

Stille coupling reaction

### ABSTRACT

9,10-Dianthryl-9,10-dihydro-9,10-diboraanthracene derivatives bearing two peripheral chloro (**3**) or bromo (**5**) substituents have been synthesized. X-ray crystallography reveals a mutually perpendicular orientation of the individual planes within each of the molecules. The two bromo substituents in **5** can be replaced by NMe<sub>2</sub> (**6**) or thiophen-2-yl (**7**) groups using Me<sub>3</sub>Sn–NMe<sub>2</sub> or *n*Bu<sub>3</sub>Sn–C<sub>4</sub>H<sub>3</sub>S and Pd-mediated C–N or C–C coupling protocols. Compounds **3**, **5**, and **7** show TICT photoluminescence and a pronounced positive solvatochromism in agreement with a charge-separated excited state.

© 2013 Elsevier Ltd. All rights reserved.

### 1. Introduction

Functional organic materials are becoming increasingly important for applications in optoelectronic devices due to their low price, light weight, high mechanical flexibility, and pronounced tunability.<sup>1</sup> Most of these materials contain extended  $\pi$ -electron systems that are composed of alkenylene, alkynylene, and/or (hetero)arylene fragments. The overall electronic properties are largely determined by the resulting conjugation lengths: Extensive conjugative interaction leads to small HOMO–LUMO gaps and, upon charge injection, to full charge delocalization. A prominent example is polyacetylene, which can be converted to the metallic state upon oxidative doping.<sup>2</sup> Disruption of conjugation, on the other hand, provides an array of electronically decoupled subunits in which the kinetics of electron transfer between multiple potential minima decides on the charge distribution. Electronic structures of this kind are realized in compounds like oligo(9,10-anthrylene)s, in which the individual  $\pi$  systems adopt mutually perpendicular conformations due to steric congestion.<sup>3,4</sup> Oligo(9,10-anthrylene)s have application potential in a variety of areas: (i) each anthryl fragment can act as two-electron acceptor and the electrostatic interaction between the individual redox centers is small. Oligo(9,10-anthrylene)s thus possess a promising

molecular design for efficient electron storage<sup>3</sup> (ii) After the oligomers have been charged with one electron per anthryl fragment, the resulting oligoanions tend to adopt high-spin states,<sup>4,5</sup> a key precondition for the occurrence of organic ferromagnetism<sup>6</sup> (iii) Oligo(9,10-anthrylene)s ( $n=2, 3, 4$ ) have shown to undergo photoinduced intramolecular charge separation in polar solvents.<sup>7</sup> The elucidation of the underlying photodynamic mechanisms is relevant for an understanding of primary processes of photosynthesis<sup>8</sup> and for the design of artificial light-harvesting systems.

As exemplified by 9,9'-bianthryl (**A**), ultraviolet excitation of the compound in a polar environment leads to an equilibrium between the nonpolar, locally excited species **A**<sup>LE</sup> and the charge-transfer species **A**<sup>CT</sup> (Fig. 1). Dual fluorescence is observed when the **A**<sup>LE</sup>/**A**<sup>CT</sup> mixture relaxes to the electronic ground state.<sup>9,10</sup> Given that the two anthryl halves of **A** are chemically equivalent (i.e., there is no natural electron donor or acceptor fragment in the molecule), the excited-state charge separation is essentially solvent-induced and consequently the CT spectrum is sensitive to the solvent configuration about the fluorophore.

Attempts have been made to increase the charge-transfer rates through the combination of polycyclic  $\pi$ -conjugated moieties with more complementary electron donor/acceptor properties. Examples are 9-(9'-anthryl)carbazole (**B**)<sup>10</sup> and 9,10-dianthryl-9,10-dihydro-9,10-diboraanthracenes **C** (Fig. 1).<sup>11</sup>

In the case of **C**-type compounds, the 9,10-dihydro-9,10-diboraanthracene (DBA) cores are isoelectronic with the extremely reactive anthracene dication.<sup>12</sup> As a result, highly efficient

\* Corresponding author. E-mail address: [Matthias.Wagner@chemie.uni-frankfurt.de](mailto:Matthias.Wagner@chemie.uni-frankfurt.de) (M. Wagner).

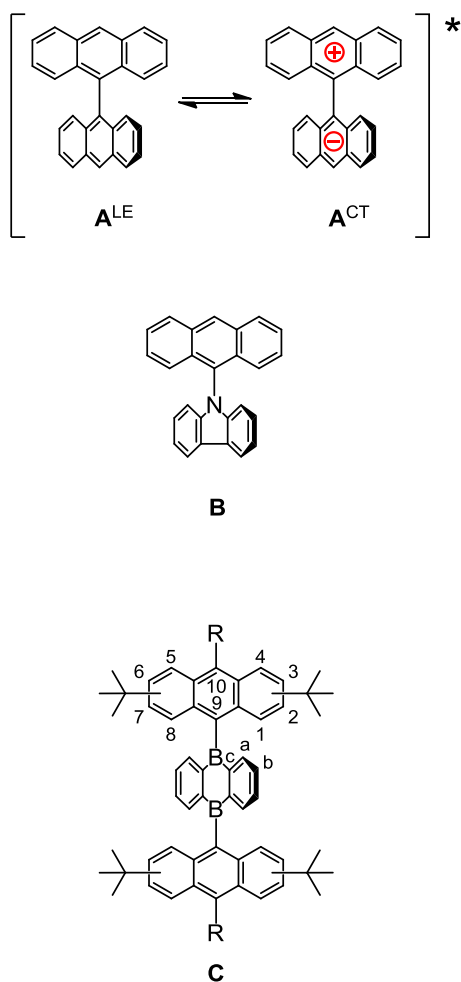


**Fig. 1.** Equilibrium between the locally excited (LE) and the charge-transfer (CT) state in electronically excited 9,9'-bianthryls **A**, 9-(9'-anthryl)carbazole **B**, and substituted 9,10-dianthryl-9,10-dihydro-9,10-diboraanthracenes **C**.

donor–acceptor–donor triads are formed, the fluorescence spectra of which show no indication of emission from locally excited anthryl states but exclusively the radiative back transition from the charge-transfer state to the ground state.<sup>11</sup> Substituents R in the 10-position of the anthryl fragments provide excellent set-screws for a fine-tuning of the emission wavelength of **C**, but also a means to incorporate **C** into more extended aggregates.

In the past, we have already introduced phenyl rings as well as dimesitylboryl and *N,N*-di(*p*-tolyl)amino groups as substituents R. All of them were attached to the anthracene scaffold prior to the final assembly of the triad.<sup>11</sup> The purpose of this paper is to describe facile routes to halogeno-substituted derivatives **C** (R=Cl, Br), which allow for an a posteriori modification of the molecule. We will show that Pd-catalyzed Stille reactions are well-suited for the replacement of R=Br by NMe<sub>2</sub> or C<sub>4</sub>H<sub>3</sub>S (thiophen-2-yl) and we will describe key optoelectronic properties of the compounds obtained.

## 2. Results and discussion

9,10-Dianthryl-DBAs (**C**) have to be equipped with alkyl side-chains in order to obtain soluble compounds. In the past, we selected *tert*-butyl (*t*Bu) groups for this purpose, because 2,6- and 2,7-di-*tert*-butylantracene are easily available and help to accomplish a compromise between good solubility and high crystallinity.<sup>11</sup> 2,6-Di-*tert*-butylantracene, however, bears the disadvantage

that the resulting 9,10-dianthryl-DBAs are formed as pairs of atropisomers.<sup>11</sup> We are therefore focusing solely on 2,7-di-*tert*-butylantracene in the present study, which will lead to compounds **C** with either four inward-pointing (located at C-2 and C-7 in Fig. 1) or four outward-pointing *t*Bu groups (located at C-3 and C-6 in Fig. 1). The selection of the preferential substitution pattern will depend on the specific case: (i) inward-pointing *t*Bu groups provide additional kinetic shielding to the boron atoms and therefore help to render the molecules stable toward air and moisture. Moreover, they stay out of the way of the substituents R, which are therefore less restricted in size. (ii) Outward-pointing *t*Bu groups offer the possibility to synthesize boron-doped graphene flakes through dehydrogenative C–C coupling reactions between the DBA core and the two anthryl fragments.<sup>13,14</sup>

Our initial attempts at the synthesis of soluble 9,10-dianthryl-DBAs bearing bromine atoms at the peripheral positions of their anthryl substituents relied on 9,10-dibromo-2,7-di-*tert*-butylantracene (9,10-Br<sub>2</sub>-2,7-DTBA) as starting material. The compound is readily available from 2,7-di-*tert*-butylantracene (2,7-DTBA)<sup>11</sup> and 2 equiv of *N*-bromosuccinimide in the presence of a catalytic amount of FeCl<sub>3</sub> (cf. Supplementary data for full details). The introduction of the anthryl substituent into the DBA core requires Li/Br exchange on 9,10-Br<sub>2</sub>-2,7-DTBA and a subsequent nucleophilic substitution reaction with 9,10-dibromo-DBA (**2**; Scheme 1). We hoped to be able to discriminate between the two bromine atoms by using 1 equiv of the sterically demanding *tert*-butyllithium in the Li/Br exchange reaction. However, after quenching of the anthryllithium reagent with H<sub>2</sub>O no preparatively useful selectivity between 9- and 10-lithiation was observed. We therefore abandoned 9,10-Br<sub>2</sub>-2,7-DTBA and turned our attention to 10-bromo-9-chloro-2,7-di-*tert*-butylantracene (**1**; Scheme 1).

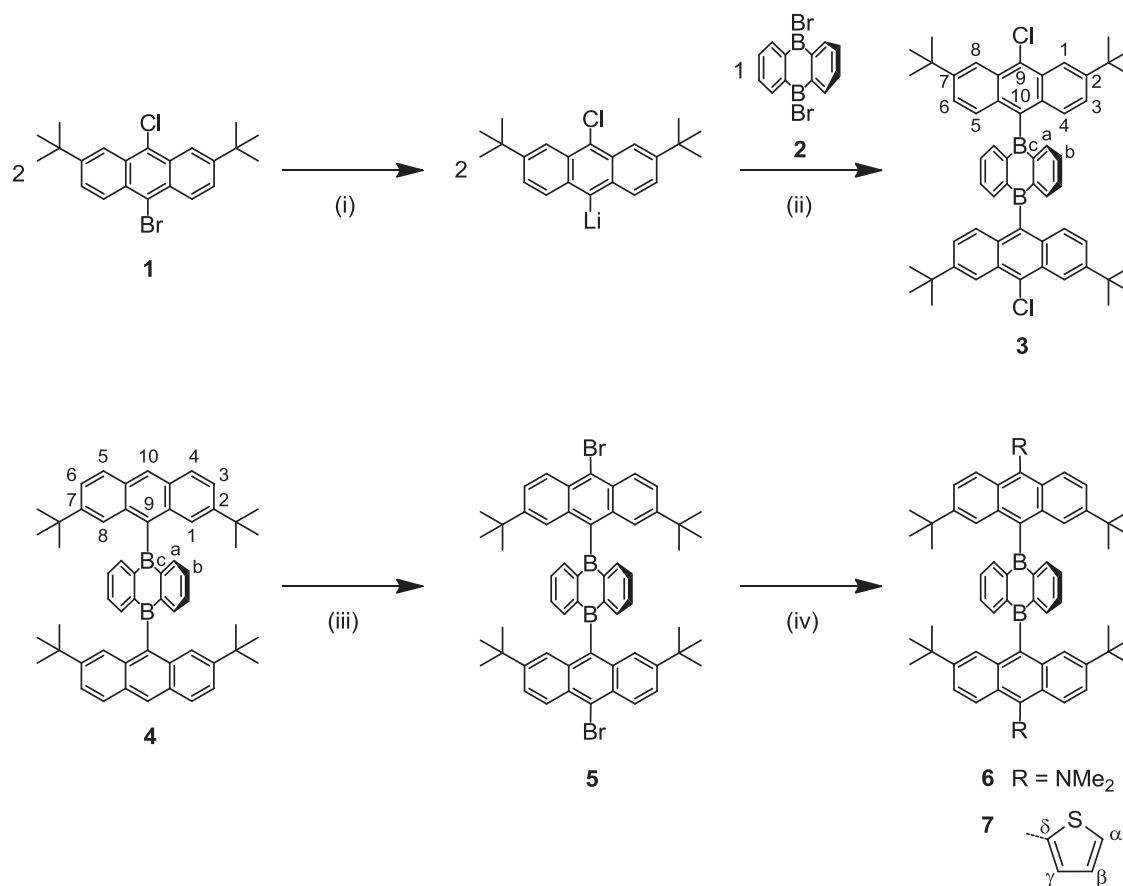
### 2.1. Dichlorinated 9,10-dianthryl-DBA with outward-pointing *tert*-butyl groups

Treatment of 2,7-DTBA<sup>11</sup> with 1 equiv of *N*-chlorosuccinimide/HCl results in the selective monochlorination at the 9-position of the anthracene scaffold (9-Cl-2,7-DTBA). 9-Cl-2,7-DTBA was subsequently transformed into **1** using *N*-bromosuccinimide/FeCl<sub>3</sub> (cf. Supplementary data for more details). Li/Br exchange with 1 equiv of *n*-butyllithium, followed by the addition of 9,10-dibromo-DBA (**2**) gave the dichlorinated 9,10-dianthryl-DBA **3** in 57% yield (Scheme 1).

The <sup>1</sup>H NMR spectrum (CDCl<sub>3</sub>) of **3** shows one singlet at 1.50 ppm (integrating 36H) for the four magnetically equivalent *t*Bu groups, two multiplets for the DBA core (7.29 ppm (4H), 7.42 ppm (4H)), and three signals for the anthryl substituents (3×4H). The <sup>13</sup>C{<sup>1</sup>H} NMR spectrum is also in full agreement with the proposed highly symmetric molecular structure; a resonance at 128.5 ppm can be assigned to the Cl-bonded carbon atom. Compound **3** does not exhibit a <sup>11</sup>B{<sup>1</sup>H} NMR resonance, likely because the signal is broadened beyond detection.

### 2.2. Difunctionalized 9,10-dianthryl-DBAs with inward-pointing *tert*-butyl groups

A seemingly straightforward strategy for the preparation of dihalogenated 9,10-dianthryl-DBAs with inward-pointing *tert*-butyl groups would be to invert the reaction sequence leading to **1**, i.e., to take 9-bromo-2,7-di-*tert*-butylantracene (9-Br-2,7-DTBA)<sup>11</sup> and treat it with *N*-chlorosuccinimide/HCl. In our hands, this approach led to product mixtures and partial Br/Cl exchange and was therefore not pursued further. Instead, we conducted an a posteriori functionalization of the 9,10-dianthryl-DBA **4**<sup>11</sup> with 2 equiv of *N*-bromosuccinimide/FeCl<sub>3</sub> to obtain the dibrominated species **5** in 90% yield (Scheme 1). An advantage of compound **5** over **3** lies in



**Scheme 1.** Synthesis of compounds **3**, **5**, **6**, and **7**. Reagents and conditions: (i) *n*BuLi (2.2 equiv), Et<sub>2</sub>O, –78 °C → rt, 1 h. (ii) Et<sub>2</sub>O–toluene, –78 °C → rt, 12 h. (iii) NBS (2 equiv), FeCl<sub>3</sub>, CHCl<sub>3</sub>, rt, 48 h. (iv) **6**: Me<sub>3</sub>Sn–NMe<sub>2</sub> (2.2 equiv), (tBu<sub>3</sub>P)<sub>2</sub>Pd, toluene, 80 °C, 24 h; **7**: *n*Bu<sub>3</sub>Sn–C<sub>4</sub>H<sub>3</sub>S (5.5 equiv), (tBu<sub>3</sub>P)<sub>2</sub>Pd, toluene, 80 °C, 48 h. NBS = *N*-bromosuccinimide.

the fact that arylbromides tend to undergo Pd-catalyzed coupling reactions more readily than arylchlorides. Given that **5** is an arylborane and that Suzuki-coupling protocols are based on the cleavage of B–C bonds, we decided against the Suzuki reaction and relied on the Stille coupling for further derivatization. The bromine atoms in **5** can efficiently be replaced by NMe<sub>2</sub> groups or thiophen-2-yl rings upon the Pd-mediated reaction with Me<sub>3</sub>Sn–NMe<sub>2</sub> or *n*Bu<sub>3</sub>Sn–C<sub>4</sub>H<sub>3</sub>S, respectively (cf. **6**, **7**; Scheme 1).

The NMR spectra (C<sub>6</sub>D<sub>6</sub>) of **5** reveal similar general features as those of the non-brominated compound **4**.<sup>11</sup> Noteworthy differences are (i) the absence of the H-10 signal in the proton spectrum of **5** and (ii) a downfield shift of the H-4,5 resonances from 8.10 ppm (**4**) to 8.87 ppm (**5**).

Upon going from **5** to **6**, NMe<sub>2</sub> signals appear at 3.38 ppm and 45.1 ppm in the <sup>1</sup>H and <sup>13</sup>C{<sup>1</sup>H} NMR spectra, respectively. The successful introduction of the amino group is further indicated by the absence of a C(aryl)–Br resonance at 123.0 ppm (**5**) and the presence of a characteristic C(aryl)–N resonance at 145.8 ppm (**6**). <sup>13</sup>C{<sup>1</sup>H} NMR spectroscopy provides a useful diagnostic tool to map the π-electron density distribution in acenes<sup>15</sup> and thereby to evaluate the donor effect of the NMe<sub>2</sub> groups on the anthryl fragments. Compared to **4**, the carbon atoms in the positions *ortho* and *para* to the NMe<sub>2</sub> substituents experience upfield shifts of only 1.5 ppm (C-4a, 10a) and 1.9 ppm (C-9), which suggests that the +M effect of the amino groups in **6** is rather small.

The <sup>1</sup>H and <sup>13</sup>C{<sup>1</sup>H} NMR spectra of the 9,10-dianthryl-DBA core of **7** do not deviate significantly from those of **4**. An H-10 signal is, however, absent in the proton spectrum of **7**; three doublets appear instead, which are assignable to the thiophen-2-yl rings (7.13, 7.29, 7.36 ppm). The corresponding <sup>13</sup>C NMR resonances

are detected at 126.9 (C-α), 127.6 (C-β), 129.7 (C-γ), and 140.6 ppm (C-δ).

### 2.3. X-ray crystal structure analyses of **3**, **5**, **6**, and **7**

Selected crystallographic data for **3**, **5**, **6**, and **7** are summarized in Tables 1 and 2.

The solid-state structure of **3** reveals two chloro substituents at C(2) and C(2A) as well as four outward-pointing *t*Bu groups (Fig. 2). Dihedral angles C(11)C(1)C(21)//C(31)B(1)C(32A) of 70.3(3)° unequivocally prove the lack of π-conjugation between the associated electron clouds. Only negligible differences are evident between the exocyclic and endocyclic B–C bond lengths and none of the bond angles about the trigonal-planar boron centers deviates by more than 1° from the ideal angle of 120°.

The dibrominated derivative **5** crystallizes from toluene with two crystallographically independent molecules in the asymmetric unit (**5**<sub>A</sub>, **5**<sub>B</sub>). Since most structural parameters of **5**<sub>A</sub> and **5**<sub>B</sub> are closely similar, only the molecular structure of **5**<sub>A</sub> is shown in Fig. 2. **5**<sub>A</sub> possesses an inversion center in the solid state, which renders the two anthryl substituents coplanar; the same is true for **5**<sub>B</sub>. The dihedral angles C(11)C(1)C(21)//C(31)B(1)C(32A) between the anthryl fragments and the DBA cores differ between **5**<sub>A</sub> (85.4(2)°) and **5**<sub>B</sub> (70.2(3)°). Moreover, the anthryl scaffolds in **5**<sub>A</sub> are significantly twisted with dihedral angles C(12)C(13)C(14)//C(22)C(23)C(24) of 16.1(7)°, whereas **5**<sub>B</sub> contains essentially planar anthryl moieties (C(12)C(13)C(14)//C(22)C(23)C(24)=0.6(8)°). The space-filling models of **5**<sub>A</sub>/**5**<sub>B</sub> clearly reveal that the vacant boron π orbitals are efficiently shielded not only by the hydrogen atoms at C(12) and C(22) but also by the *t*Bu groups. We find B(1)–C(1) bond

**Table 1**  
Crystallographic data for **3** and **5**

	<b>3</b>	<b>5</b>
Formula	C <sub>56</sub> H <sub>56</sub> B <sub>2</sub> Cl <sub>2</sub> ×4 CHCl <sub>3</sub>	C <sub>56</sub> H <sub>56</sub> B <sub>2</sub> Br <sub>2</sub> ×1.5 C <sub>7</sub> H <sub>8</sub>
M <sub>r</sub>	1299.00	1048.65
Color, shape	Red, block	Red, plate
T [K]	173(2)	173(2)
Radiation, λ [Å]	MoKα, 0.71073	MoKα, 0.71073
Crystal system	Monoclinic	Triclinic
Space group	P2 <sub>1</sub> /c	P-1
a [Å]	14.7190(7)	9.9122(10)
b [Å]	9.0634(7)	15.0820(13)
c [Å]	23.9955(12)	19.324(2)
α [°]	90	79.074(8)
β [°]	91.331(4)	84.207(8)
γ [°]	90	77.152(8)
V [Å <sup>3</sup> ]	3200.2(3)	2760.3(5)
Z	2	2
D <sub>calcd</sub> [g cm <sup>-3</sup> ]	1.348	1.262
F(000)	1336	1094
μ [mm <sup>-1</sup> ]	0.639	1.509
Crystal size [mm <sup>3</sup> ]	0.42×0.38×0.22	0.49×0.28×0.07
Rfins collected	38,217	35,615
Independent rfins (R <sub>int</sub> )	5647 (0.0895)	10,373 (0.1020)
Data/restraints/parameters	5647/0/343	10,373/19/637
GOF on F <sup>2</sup>	1.077	1.013
R <sub>1</sub> , wR <sub>2</sub> [I>2σ(I)]	0.0858, 0.2316	0.0604, 0.1090
R <sub>1</sub> , wR <sub>2</sub> (all data)	0.1071, 0.2461	0.1050, 0.1219
Largest diff peak and hole [e Å <sup>-3</sup> ]	1.255, -1.018	0.625, -0.353

**Table 2**  
Crystallographic data for **6** and **7**

	<b>6</b>	<b>7</b>
Formula	C <sub>60</sub> H <sub>68</sub> B <sub>2</sub> N <sub>2</sub>	C <sub>64</sub> H <sub>62</sub> B <sub>2</sub> S <sub>2</sub> ×2.5 C <sub>6</sub> H <sub>6</sub>
M <sub>r</sub>	838.78	1112.14
Color, shape	Gray, plate	Red, block
T [K]	173(2)	173(2)
Radiation, λ [Å]	MoKα, 0.71073	MoKα, 0.71073
Crystal system	Monoclinic	Triclinic
Space group	P2 <sub>1</sub> /c	P-1
a [Å]	9.1712(12)	15.2919(9)
b [Å]	25.295(2)	15.3394(9)
c [Å]	10.6954(13)	16.6380(10)
α [°]	90	72.752(4)
β [°]	94.101(10)	85.225(5)
γ [°]	90	60.642(4)
V [Å <sup>3</sup> ]	2474.8(5)	3239.5(4)
Z	2	2
D <sub>calcd</sub> [g cm <sup>-3</sup> ]	1.126	1.140
F(000)	904	1186
μ [mm <sup>-1</sup> ]	0.063	0.126
Crystal size [mm <sup>3</sup> ]	0.50×0.25×0.15	0.60×0.55×0.53
Rfins collected	27,406	43,588
Independent rfins (R <sub>int</sub> )	5062 (0.1582)	12,449 (0.0397)
Data/restraints/parameters	5062/0/292	12,449/18/746
GOF on F <sup>2</sup>	1.008	1.034
R <sub>1</sub> , wR <sub>2</sub> [I>2σ(I)]	0.0784, 0.1370	0.0630, 0.1635
R <sub>1</sub> , wR <sub>2</sub> (all data)	0.1561, 0.1642	0.0802, 0.1738
Largest diff peak and hole [e Å <sup>-3</sup> ]	0.197, -0.277	0.540, -0.461

lengths of 1.594(5) Å in **5<sub>A</sub>** and 1.587(5) Å in **5<sub>B</sub>**, which can be compared with an exocyclic B–C bond length of 1.577(7) Å in **4<sup>11</sup>** or 1.575(6) Å in the sterically less congested chloro-derivative **3**. We therefore conclude that neither the presence of electronegative substituents at C(2) nor the positions of the *t*Bu substituents (i.e., inward- vs outward-pointing) have a systematic influence on the B(1)–C(1) bonds.

The solid-state structure of **6** (Fig. 3) shows an anthryl twist (C(12)C(13)C(14)//C(22)C(23)C(24)=14.9(6)°) reminiscent of **5<sub>A</sub>**. At the same time, the anthryl moieties deviate substantially from a position perpendicular to the DBA core (C(11)C(1)C(21)//C(31)B(1)C(32A)=71.9(1)°), as it has already been observed for **5<sub>B</sub>**.

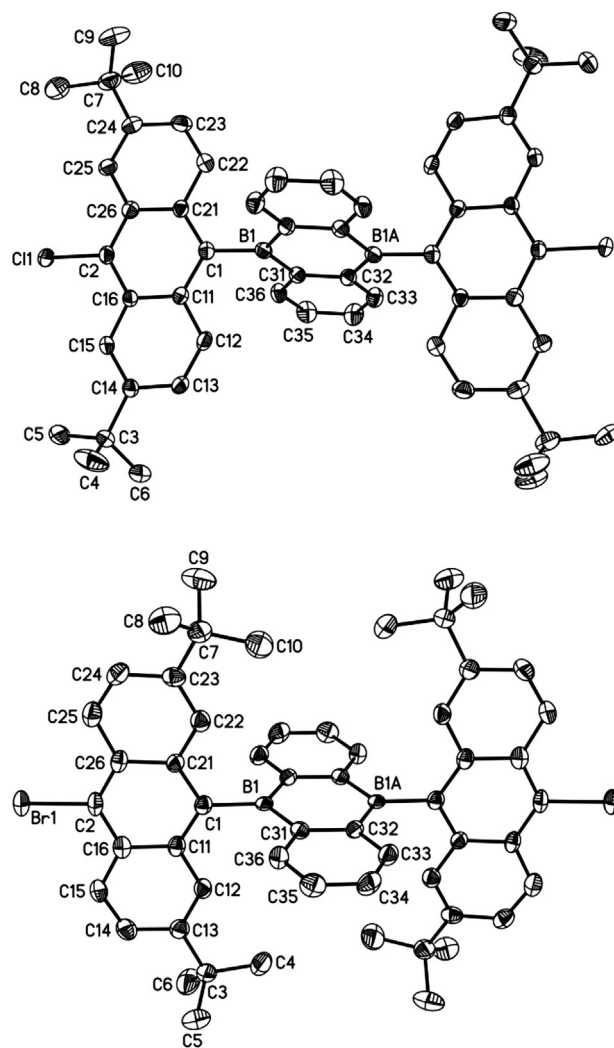


**Fig. 2.** Molecular structures of **3** (top) and **5<sub>A</sub>** (bottom) in the solid state; displacement ellipsoids at the 50% probability level, H atoms omitted for clarity. Selected bond lengths (Å), bond angles (deg), and dihedral angle (deg): **3**: C(1)–C(2) 1.747(4), B(1)–C(1) 1.575(6), B(1)–C(31) 1.566(6), B(1)–C(32A) 1.555(6), C(31)–C(32) 1.431(5); C(1)–B(1)–C(31) 119.0(3), C(1)–B(1)–C(32A) 121.0(3), C(31)–B(1)–C(32A) 120.0(3); C(11)C(1)C(21)//C(31)B(1)C(32A) 70.3(3). Symmetry transformation used to generate equivalent atoms: A:  $-x+1, -y, -z+1$ . **5<sub>A</sub>**: Br(1)–C(2) 1.909(3), B(1)–C(1) 1.594(5), B(1)–C(31) 1.556(6), B(1)–C(32A) 1.551(6), C(31)–C(32) 1.423(5); C(1)–B(1)–C(31) 121.1(3), C(1)–B(1)–C(32A) 119.3(3), C(31)–B(1)–C(32A) 119.6(3); C(11)C(1)C(21)//C(31)B(1)C(32A) 85.4(2). Symmetry transformation used to generate equivalent atoms: A:  $-x+1, -y+1, -z+1$ .

Likely for steric reasons, the NMe<sub>2</sub> group does not lie in the plane of its respective anthryl fragment. We observe a concomitant disorder of the NMe<sub>2</sub> groups indicating that a proportion of 60% adopts a pyramidalized configuration and only 40% are planar. The dihedral angle between the planar NMe<sub>2</sub> moieties and their adjacent anthryl groups is around 60°. The N(1)–C(2) bond length amounts to 1.418(4) Å and is thus considerably larger than comparable Me<sub>2</sub>N–C(phenyl) bond lengths in a variety of *N,N*-dimethylaniline derivatives with in-plane amino groups (1.375–1.388 Å).<sup>16</sup> Our crystallographic results therefore support the previous interpretation of the <sup>13</sup>C{<sup>1</sup>H} NMR spectrum of **6**, namely, that the NMe<sub>2</sub> substituents in **6** do not exert their full π-donor capacity.

The crystal lattice of the thienyl derivative **7** also contains two crystallographically independent molecules in the asymmetric unit (**7<sub>A</sub>**, **7<sub>B</sub>**; cf. Fig. 3 for a plot of **7<sub>A</sub>**). Both molecules are centrosymmetric; the dihedral angles between the thiophen-2-yl rings and their respective 9,10-anthrylene moieties amount to 79.3(1)° (**7<sub>A</sub>**) and 85.8(2)° (**7<sub>B</sub>**). All other key structural parameters of **7<sub>A</sub>** and **7<sub>B</sub>**

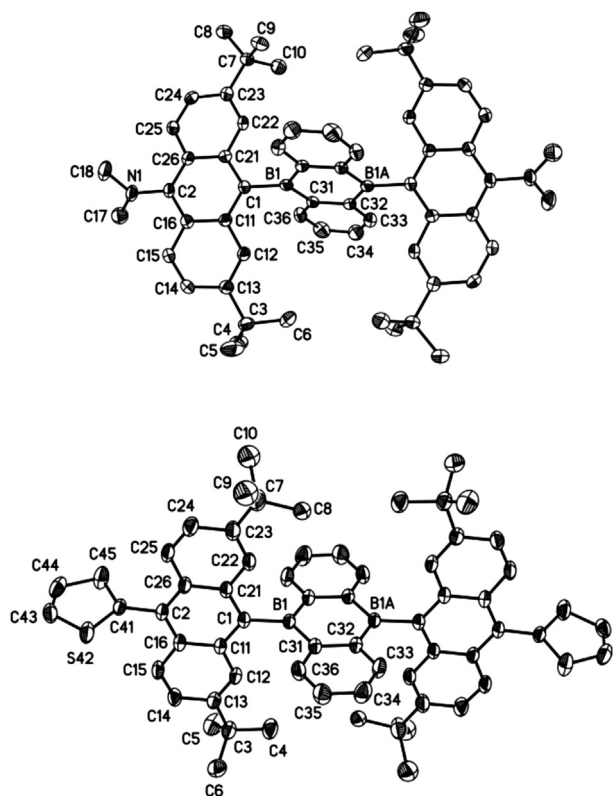


**Fig. 3.** Molecular structure of **6** (top) and **7<sub>A</sub>** (bottom) in the solid state; displacement ellipsoids at the 50% probability level, H atoms omitted for clarity. Selected bond lengths (Å), bond angles (deg), and dihedral angles (deg): **6**: N(1)–C(2) 1.418(4), B(1)–C(1) 1.575(4), B(1)–C(31) 1.561(4), B(1)–C(32A) 1.562(4), C(31)–C(32) 1.418(4); C(1)–B(1)–C(31) 120.2(3), C(1)–B(1)–C(32A) 120.5(3), C(31)–B(1)–C(32A) 119.2(2); C(11)C(1)C(21)/C(31)B(1)C(32A) 71.9(1), C(16)C(2)C(26)/C(17)N(1)C(18) 60.2(4). Symmetry transformation used to generate equivalent atoms: A:  $-x+1, -y+1, -z+1$ . **7<sub>A</sub>**: B(1)–C(1) 1.589(3), B(1)–C(31) 1.556(3), B(1)–C(32A) 1.557(3), C(2)–C(41) 1.480(3), C(31)–C(32) 1.426(3); C(1)–B(1)–C(31) 122.0(2), C(1)–B(1)–C(32A) 119.4(2), C(31)–B(1)–C(32A) 118.6(2); C(11)C(1)C(21)/C(31)B(1)C(32A) 85.4(2), C(16)C(2)C(26)/S(42)C(41)C(45) 79.3(1). Symmetry transformation used to generate equivalent atoms: A:  $-x+2, -y, -z$ .

are similar to those of the previously discussed molecules and therefore do not require a detailed discussion.

#### 2.4. Electrochemical investigation of **6** and **7**

Compounds **6** and **7** were further characterized by cyclic voltammetry (THF,  $[n\text{Bu}_4\text{N}][\text{PF}_6]$  (0.1 M), vs ferrocene/ferrocenium (Fch/Fch<sup>+</sup>)). The redox potentials are compiled in Table 3.

**Table 3**  
Electrochemical data of **6** and **7**<sup>a</sup>

	$E_{1/2}$ in [V] versus Fch/Fch <sup>+</sup>	
	Oxidation	Reduction
<b>6</b>	+0.23 <sup>b</sup>	–1.77, –2.60, –3.30 <sup>c</sup>
<b>7</b>	—	–1.69, –2.50, –3.10 <sup>c</sup> , –3.40 <sup>c</sup>

<sup>a</sup> THF, supporting electrolyte:  $[n\text{Bu}_4\text{N}][\text{PF}_6]$  (0.1 M), scan rate: 200 mV s<sup>–1</sup>.

<sup>b</sup>  $E_{\text{pa}}$  value.

<sup>c</sup>  $E_{\text{pc}}$  value.

Compound **6** undergoes an irreversible oxidation process at  $E_{\text{pa}}=+0.23$  V. A second ill-defined feature appears at slightly more anodic potential values (Fig. 4). In the cathodic regime, two reversible redox waves are observed at  $E_{1/2}=-1.77$  and  $-2.60$  V. An assignment of these waves as DBA-centered was achieved by comparison with the corresponding redox potentials of compound **4** ( $E_{1/2}=-1.73, -2.57$  V)<sup>11</sup> and by UV/vis spectroelectrochemistry:

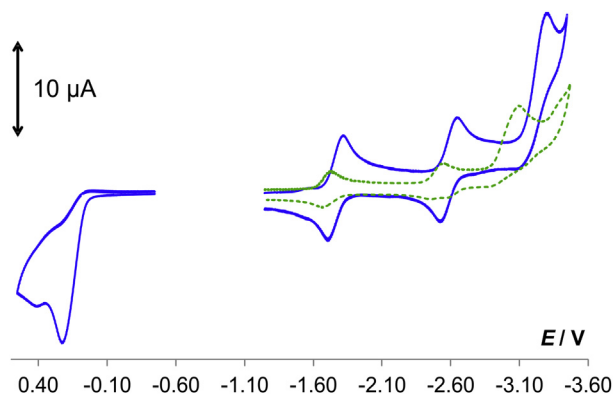


**Fig. 4.** Cyclic voltammograms of **6** (solid line) and **7** (dashed line). THF solutions, rt,  $[n\text{Bu}_4\text{N}][\text{PF}_6]$  (0.1 M), scan rate 200 mV s<sup>–1</sup>, versus Fch/Fch<sup>+</sup>.

chemical reduction of **6** with elemental potassium first led to the characteristic UV/vis signature of the DBA monoanion ( $\lambda_{\text{max}}=539, 750, 835, 945$  nm).<sup>11,17</sup> Within hours, these bands gradually vanished and new absorptions developed at  $\lambda_{\text{max}}=474$  and 665 nm, which are attributable to the DBA dianion (cf. Supplementary data for plots of the UV/vis spectra).<sup>11,17</sup> A third, irreversible reduction event occurs in the cyclic voltammogram of **6** at a peak potential of  $E_{\text{pc}}=-3.30$  V. Compared to the anthryl reduction of **4** ( $E_{\text{pc}}=-3.21$  V) there is only a minor cathodic shift, again indicating that the +M effect of the NMe<sub>2</sub> substituents is small.

In the case of **7**, DBA reduction takes place at potential values  $E_{1/2}$  of  $-1.69$  and  $-2.50$  V; these transitions are reversible as long as the switching potential is not taken below  $-2.8$  V (cf. Supplementary data for more information). Two additional irreversible redox waves are visible at  $E_{\text{pc}}=-3.10$  and  $-3.40$  V.

#### 2.5. Optical properties of **3**, **5**, **6**, and **7**

Table 4 summarizes key UV/vis absorption and emission data of the 9,10-dianthryl-DBAs under investigation here. Because of the poor solubility of **3** in C<sub>6</sub>H<sub>12</sub>, C<sub>6</sub>H<sub>6</sub>, and CH<sub>2</sub>Cl<sub>2</sub>, measurements on this compound were limited to the solvent CHCl<sub>3</sub>. The UV/vis spectra of **3** and **5** in CHCl<sub>3</sub> are essentially identical, each of them showing two absorption bands. The respective short-wavelength band at  $\lambda_{\text{max}}=377$  nm has a vibrational fine structure and a similar position and line shape as the 2,7-DTBA absorption.<sup>11</sup> It is therefore likely attributable to a local  $\pi-\pi^*$  electron transition within the anthryl systems. A broad, featureless second band is observed at  $\lambda_{\text{max}}=510$  nm both in the absorption spectrum of **3** and of **5**. We assign this band to a charge-transfer transition from the

**Table 4**  
UV/vis absorption and emission data of **3**, **5**, **6**, and **7**

	Solvent	$\lambda_{\text{max}}(\text{abs})$ [nm] ( $\epsilon$ [mol <sup>–1</sup> dm <sup>3</sup> cm <sup>–1</sup> ])	$\lambda_{\text{max}}(\text{em})$ [nm] ( $\lambda_{\text{ex}}$ [nm])		$\phi_{\text{F}}^{\text{a}}$
<b>3</b>	CHCl <sub>3</sub>	377 (17,000), 510 (1400)	655 (520)		0.03
<b>5</b>	C <sub>6</sub> H <sub>12</sub>	375 (18,900), 548 (2100)	567 (520)		0.03
	CHCl <sub>3</sub>	377 (20,800), 510 (2000)	640 (520)		0.02
<b>6</b>	C <sub>6</sub> H <sub>12</sub>	371 (23,200), 567 (3400)	—		—
	C <sub>6</sub> H <sub>6</sub>	371 (25,600), 546 (2600)	—		—
<b>7</b>	C <sub>6</sub> H <sub>12</sub>	373 (21,700), 557 (2300)	582 (520)		0.11
	C <sub>6</sub> H <sub>6</sub>	375 (25,000), 521 (1600)	624 (520)		0.09
	THF	374 (22,100), 525 (1500)	680 (520)		0.04
	CH <sub>2</sub> Cl <sub>2</sub>	376 (28,500), 521 (2300)	700 (520)		0.03

<sup>a</sup> Quantum yields were determined using a calibrated integration sphere; excitation in the long-wavelength absorption band.

more electron-rich anthryl donor to the electron-poor DBA acceptor. This band is responsible for the red color of the compounds.

The fluorescence spectra of **3** and **5** exhibit broad emissions at  $\lambda_{\text{max}}=655$  and  $640$  nm ( $\text{CHCl}_3$ ), respectively, when the molecules are excited either at  $\lambda_{\text{ex}}=366$  nm (anthryl absorption) or  $\lambda_{\text{ex}}=520$  nm (charge-transfer transition).

In summary, neither the nature of the halogeno substituent (**3**: Cl; **5**: Br), nor the position of the *t*Bu groups (**3**: outward-pointing; **5**: inward-pointing) has a noteworthy effect on the absorption or emission behavior of these 9,10-dianthryl-DBAs.

In  $\text{C}_6\text{H}_6$  solution, compound **6** (Fig. 5) shows two analogously shaped absorptions as **3** and **5**, i.e., a hypsochromic band at  $\lambda_{\text{max}}=371$  nm and a bathochromic band at  $\lambda_{\text{max}}=546$  nm. The latter is remarkably red-shifted compared to **4** ( $\lambda_{\text{max}}=510$  nm).<sup>11</sup> Neither in solution nor in the solid state does compound **6** give rise to an appreciable fluorescence. A possible explanation could be the well-known quenching effect of amines on anthracenes.<sup>18</sup> We therefore added 2 equiv of ethereal HCl to a solution of **6** in  $\text{THF-d}_8$  in an attempt to sequester the nitrogen lone pairs. As a result, the  $\text{NMe}_2$  proton resonances underwent a downfield shift of 0.17 ppm, the anthryl H-3,6 signals of 0.11 ppm, and the anthryl H-4,5 resonances of 0.32 ppm. Moreover, a broad hump at 9.88 ppm, integrating approximately 2H, appeared in the  $^1\text{H}$  NMR spectrum (cf. Supplementary data for plots of the spectra before and after the addition of  $\text{HCl}\cdot\text{Et}_2\text{O}$ ). Nevertheless, the solution remained non-fluorescent. We therefore assume that the protonation/deprotonation equilibrium is not sufficiently shifted to the side of the ammonium species to suppress the amine quenching effect.

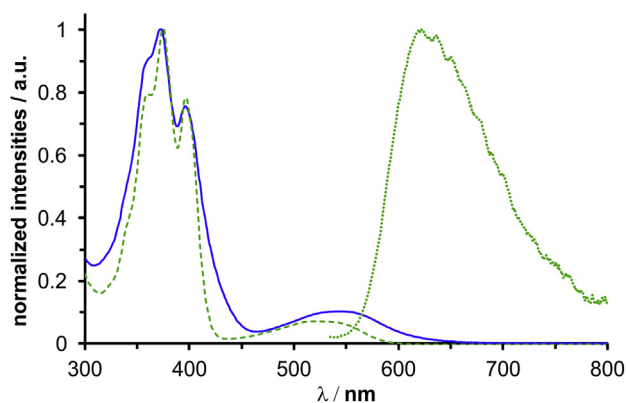


Fig. 5. UV/vis absorption spectra of **6** (solid line) and **7** (dashed line); UV/vis emission spectrum (dotted line) of **7**;  $\text{C}_6\text{H}_6$  solutions.

An addition of excess  $\text{HCl}\cdot\text{Et}_2\text{O}$  is not advisable, because this leads to extensive protolysis of the molecular framework. Interestingly, the closely related 9,10-dianthryl-DBA derivative bearing  $\text{NTol}_2$  instead of  $\text{NMe}_2$  substituents is also essentially non-fluorescent in solution, but emits bright wine-red light in the solid state ( $\text{Tol}=p\text{-tolyl}$ ).<sup>11</sup>

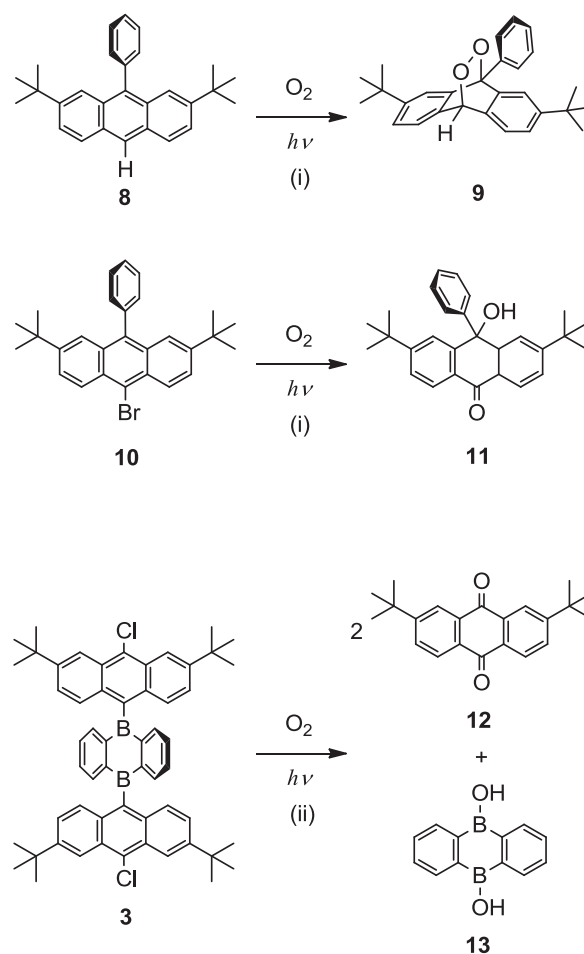
The two absorption bands of the thiophen-2-yl derivative **7** in  $\text{C}_6\text{H}_6$  are red-shifted by about 10 nm compared to those of **4**. The fluorescence bands of **7** are strongly influenced by the solvent polarity ( $\lambda_{\text{em}}=582$  ( $\text{C}_6\text{H}_{12}$ ),  $624$  ( $\text{C}_6\text{H}_6$ ),  $680$  (THF), and  $700$  nm ( $\text{CH}_2\text{Cl}_2$ )), in line with the postulated charge-separated excited state (cf.  $\text{A}^{\text{CT}}$  in Fig. 1). The positive solvatochromism of **7** is accompanied by a decrease in the quantum yield, i.e.,  $\phi_{\text{F}}=0.11$  ( $\text{C}_6\text{H}_{12}$ ),  $0.09$  ( $\text{C}_6\text{H}_6$ ),  $0.04$  (THF), and  $0.03$  ( $\text{CH}_2\text{Cl}_2$ ).

## 2.6. Oxidative degradation of 9,10-dianthryl-DBAs

As already noted in a previous publication,<sup>11</sup> 9,10-dianthryl-DBAs **C** (Fig. 1) are pleasingly stable toward moisture. Targeted

hydrolysis studies usually provide first indications of decomposition not earlier than 6 h after the addition of  $\text{H}_2\text{O}$  (NMR spectroscopic control). Fluorescence spectroscopy, however, which is even more revealing than NMR spectroscopy because the samples are more dilute by several orders of magnitude, often shows a weak emission band already soon after sample preparation, which does not belong to the actual **C**-type derivative. In the case of **C** ( $\text{R}=\text{Ph}$ ; all *tert*-butyl groups outward-pointing), this band appeared at  $\lambda_{\text{em}}=440$  nm upon irradiation into the anthryl absorption and gained in intensity in spectra taken after the closed cuvette had been left standing for extended periods of time outside the glove box or if air and moisture had been deliberately admitted.

The slow degradation of **C** ( $\text{R}=\text{Ph}$ ; all *tert*-butyl groups outward-pointing) in the presence of air and moisture leads to complex reaction mixtures rather than to the exclusive formation of the expected hydrolysis products 9,10-dihydroxy-DBA (cf. **13**; Scheme 2) and 9-phenyl-2,7-di-*tert*-butylantracene (cf. **8**; Scheme 2). We



Scheme 2. Photooxidation reactions of **8** and **10** yielding the endoperoxide **9** and the anthrone **11**, respectively; decomposition of **3** in non-dried, non-degassed  $\text{CDCl}_3$  to give the anthraquinone **12** and the boronic acid **13**. Schematic sketch of the proposed key intermediate of the degradation reaction of **3**. Reagents and conditions: (i) rose bengal/18-crown-6,  $\text{CH}_2\text{Cl}_2$ , rt, 24 h. (ii)  $\text{CDCl}_3$ , rt, 3 d.

therefore arrived at the working hypothesis that the initial degradation step more likely involves the formation of an endoperoxide at one of the anthryl moieties than the attack of water on the vacant boron p orbital. Anthracene endoperoxides are readily obtained when anthracenes are exposed to light and air: In the first step, singlet oxygen ( $^1O_2$ ) is generated, which then undergoes a cycloaddition reaction at the central six-membered ring of the anthracene molecule.<sup>19</sup>

To test this hypothesis, we irradiated an  $O_2$ -saturated  $CH_2Cl_2$  solution of **8** in the presence of air with a fluorescent lamp (9 W, we also added the photosensitizer rose bengal to boost the formation of  $^1O_2$ ; Scheme 2). After 24 h, the endoperoxide **9** was isolated in 63% yield after chromatographic workup, thereby indicating that the substitution pattern present in **C** (R=Ph; all *tert*-butyl groups outward-pointing) is compatible with the photooxidation reaction (cf. Supplementary data for more details).

We next repeated the experiment using 10-bromo-9-phenyl-2,7-di-*tert*-butylantracene as the starting material (**10**; Scheme 2). This time, the endoperoxide was not stable but reacted further to give 9-hydroxy-9-phenyl-2,7-di-*tert*-butylanthrone as the final product (**11**; cf. Supplementary data for more details including an X-ray crystal structure analysis of **11**).

The fact that halogenated anthracenes give the corresponding stable anthrones upon reaction with  $^1O_2$ , prompted us to finally select the chlorinated 9,10-dianthryl-DBA **3** for a thorough investigation of its hydrolysis/photooxidation products. After a solution of **3** in non-dried, non-degassed  $CDCl_3$  had been kept under ambient light for 3 d, the starting material had completely vanished and two new compounds had appeared instead in a stoichiometric ratio of 1:2 (NMR spectroscopic control). The first of these products was the literature-known borinic acid **13** (Scheme 2),<sup>20</sup> while the NMR signature of the other was identical with that of an authentic sample of 2,7-di-*tert*-butylantracene-9,10-dione (**12**; Scheme 2; cf. Supplementary data for more details). The formation of **12** unequivocally proves that an oxidation step rather than mere hydrolysis is responsible for the degradation of **3**. As illustrated in Scheme 2, we propose that photooxidation of **3** (which also acts as the photosensitizer) first generates an endoperoxide. As a result, the anthryl plane is bent away from its original position, thus leaving room for the nucleophilic attack of a water molecule on the boron atom with concomitant rupture of the exocyclic B–C bond and liberation of **12**. We wish to emphasize that the photooxidative decomposition of C-type 9,10-dianthryl-DBAs is therefore not a specific problem of the boron-containing species, because conventional all-carbon tri(9,10-anthrylene)s do also form endoperoxides under comparable conditions.

### 3. Conclusions

To summarize, we have prepared soluble 9,10-dianthryl-9,10-dihydro-9,10-diboraanthracene derivatives equipped with two peripheral chloro (**3**) or bromo (**5**) substituents. As expected, the individual  $\pi$  systems constituting **3** and **5** adopt mutually perpendicular conformations. Charge-transfer interactions are observed between the anthryl substituents and the 9,10-dihydro-9,10-diboraanthracene (DBA) cores, which are more pronounced than in the cases of the analogous all-carbon tri(9,10-anthrylene)s, because DBA is a strong electron acceptor. The bromine atoms in **5** can be replaced by other substituents (e.g.,  $NMe_2$  (**6**), thiophen-2-yl (**7**)) through Pd-mediated Stille coupling reactions. Compound **6** possesses a very dark color and is non-emissive in solution or the solid state, whereas the red-purple compound **7** shows an orange fluorescence ( $C_6H_{12}$ ) and pronounced positive solvatochromism in solution. The selection of suitable substituents therefore provides a powerful set-screw for the fine-tuning of the  $\pi$ -donor sets and, in turn, the optoelectronic properties of the donor–acceptor–donor triads.

## 4. Experimental section

### 4.1. General materials and methods

Unless otherwise specified, all reactions were carried out under dry nitrogen or argon using carefully dried and degassed solvents, flame-dried glassware and Schlenk or glove box techniques. Toluene, hexane, and  $C_6D_6$  were dried over Na/benzophenone.  $CHCl_3$  and  $CDCl_3$  were washed with water (eight times), dried first over  $MgSO_4$ , then over  $CaH_2$ , and freshly distilled prior to use. Solvents used for UV/vis spectroscopic measurements were purchased as spectroscopic grade ( $C_6H_{12}$ ,  $C_6H_6$ , THF,  $CHCl_3$ ,  $CH_2Cl_2$ ) and degassed prior to use. Column chromatography was performed using silica gel 60 (Macherey–Nagel). NMR spectra were recorded with Bruker Avance 300 or Avance 400 spectrometers at rt. Chemical shifts are referenced to (residual) solvent signals ( $^1H/^{13}C\{^1H\}$ ;  $C_6D_6$ :  $\delta=7.16/128.06$ ,  $CDCl_3$ :  $\delta=7.26/77.16$ ) or external  $BF_3 \cdot Et_2O$  ( $^{11}B$ ,  $^{11}B\{^1H\}$ ). Abbreviations: s=singlet, d=doublet, dd=doublet of doublets, vt=virtual triplet, m=multiplet, n.o.=not observed. Electrochemical measurements were performed at rt by using an EG&G Princeton Applied Research 263A potentiostat with a platinum disc working electrode (diameter 2.00 mm). The reference electrode was a silver wire on which AgCl had been deposited by immersing the wire into HCl/ $HNO_3$  (3:1). The solvent (THF) was dried over Na/K alloy without added benzophenone at rt and degassed first by five freeze–pump–thaw cycles and then by bubbling helium through it (40 min).  $[nBu_4N][PF_6]$  (0.1 M) was employed as the supporting electrolyte. All potential values are referenced against the ferrocene/ferrocenium couple ( $E_{1/2}=0$  V). UV/vis absorption spectra were recorded with a Varian Cary 50 Scan UV/vis spectrophotometer; for in situ UV/vis monitoring experiments an immersion probe from Hellma (10.00 mm) was employed. UV/vis emission spectra were recorded with a Spectrofluorometer FP-8300 (Jasco). The absolute fluorescence quantum yields ( $\phi_F$ ) were determined using a calibrated integrating sphere system (ILF-835 100 mm diameter Integrating Sphere; Jasco), a quantum yield calculation program (FWQE-880; Jasco) and highly diluted samples of ten different optical densities in each measurement. Mass spectra were recorded with a Fisons Instruments VG ToFSpec mass spectrometer. Combustion analyses were performed by the Microanalytical Laboratory of the Goethe-University Frankfurt.

### 4.2. Synthesis protocols and characterization data

**4.2.1. Synthesis of 3.** *n*BuLi in hexane (1.17 M, 1.2 mL, 1.4 mmol) was diluted with hexane (3 mL) and added dropwise with stirring at  $-78$  °C to a solution of **1** (500 mg, 1.24 mmol) in  $Et_2O$  (40 mL). Stirring was continued for 15 min before the reaction mixture was warmed to rt within 1 h. The resulting turbid solution was cooled to  $-78$  °C again, **2** (197 mg, 0.590 mmol) in toluene (25 mL) was added dropwise with stirring, the reaction mixture was allowed to warm to rt overnight, and all volatiles were removed under reduced pressure. The crude product was washed with non-dried  $C_6H_6$  (3 $\times$ 5 mL), non-dried MeOH (3 $\times$ 5 mL), cold non-dried  $CH_2Cl_2$  (2 $\times$ 2 mL), and non-dried pentane (3 $\times$ 5 mL). Yield: 278 mg (57%). Both in solution and in the solid state, **3** shows an intense red fluorescence when irradiated with UV light ( $\lambda_{ex}=366$  nm). Red blocks of **3** suitable for an X-ray crystal structure analysis were grown by gas-phase diffusion of hexane into a concentrated  $CHCl_3$  solution.

$^1H$  NMR (400.1 MHz,  $CDCl_3$ ):  $\delta=1.50$  (s, 36H,  $C(CH_3)_3$ ), 7.29 (m, 4H, H-b), 7.42 (m, 4H, H-a), 7.46 (dd,  $J=9.0, 1.8$  Hz, 4H, H-3,6), 7.64 (d,  $J=9.0$  Hz, 4H, H-4,5), 8.53 (d,  $J=1.8$  Hz, 4H, H-1,8);  $^{11}B\{^1H\}$  NMR (96.3 MHz,  $CDCl_3$ ):  $\delta=n. o.$  ppm;  $^{13}C\{^1H\}$  NMR (100.6 MHz,  $CDCl_3$ ):  $\delta=31.2$  ( $C(CH_3)_3$ ), 35.6 ( $C(CH_3)_3$ ), 119.6 (C-1,8), 124.3 (C-3,6), 128.5 (C-8a,9a), 128.5 (C-9), 130.0 (C-4,5), 132.5 (4a,10a), 134.3 (C-b), 140.5

(C-a), 140.5\* (C-10), 146.0\* (C-c) 149.1 (C-2,7); MS (MALDI):  $m/z$  (%): 821 (100) [ $M^+$ ]; elemental analysis calcd (%) for  $C_{56}H_{56}B_2Cl_2$  (821.57): C 81.87, H 6.87; found: C 81.42, H 6.83. \*This signal was broadened beyond detection in the  $^{13}C\{^1H\}$  NMR spectrum; its chemical shift value was determined by using the cross peak in the HSQC or HMBC spectrum.

**4.2.2. Synthesis of 5.** A suspension of *N*-bromosuccinimide (236 mg, 1.33 mmol), **4** (500 mg, 0.664 mmol), and  $FeCl_3$  (11 mg, 0.068 mmol) in  $CHCl_3$  (50 mL) was stirred at rt for 2 d. The succinimide was removed by filtration, the filtrate was evaporated to dryness in vacuo, and the resulting solid crude product was washed with non-dried MeOH ( $3 \times 5$  mL) to obtain **5** as a deep-red solid. Yield: 545 mg (90%). Both in solution and in the solid state, **5** shows an intense red fluorescence when irradiated with UV light ( $\lambda_{ex}=366$  nm). Red plates of **5** suitable for X-ray crystallography were grown by gas-phase diffusion of hexane into a concentrated toluene solution.

$^1H$  NMR (400.1 MHz,  $C_6D_6$ ):  $\delta=1.19$  (s, 36H,  $C(CH_3)_3$ ), 6.76 (m, 4H, H-b), 7.50 (m, 4H, H-a), 7.56 (dd,  $J=9.2, 1.8$  Hz, 4H, H-3,6), 7.93 (d,  $J=1.8$  Hz, 4H, H-1,8), 8.87 (d,  $J=9.2$  Hz, 4H, H-4,5);  $^{11}B\{^1H\}$  NMR (96.3 MHz,  $C_6D_6$ ):  $\delta=\sim 75$  ppm ( $h_{1/2}=3500$  Hz);  $^{13}C\{^1H\}$  NMR (75.4 MHz,  $C_6D_6$ ):  $\delta=31.1$  ( $C(CH_3)_3$ ), 34.8 ( $C(CH_3)_3$ ), 123.0 (C-10), 125.4 (C-1,8), 126.6 (C-3,6), 128.6 (C-4,5), 129.3 (4a,10a), 134.4 (C-b), 135.8 (C-8a,9a), 140.9 (C-a), 142.4 (C-9), 146.1 (C-c), 147.3 (C-2,7); MS (MALDI):  $m/z$  (%): 910 (100) [ $M^+$ ]; elemental analysis calcd (%) for  $C_{56}H_{56}B_2Br_2$  (910.47): C 73.87, H 6.20; found: C 73.77, H 6.34.

**4.2.3. Synthesis of 6.** Neat  $Me_3Sn-NMe_2$  (50.2 mg, 241  $\mu$ mol) was added to a solution of **5** (100 mg, 110  $\mu$ mol) and  $(tBu_3P)_2Pd$  (4.5 mg, 8.8  $\mu$ mol) in toluene (5 mL). The mixture was heated at 80 °C for 24 h. After cooling to rt, the insolubles were removed by filtration, washed with non-dried  $CHCl_3$  ( $3 \times 5$  mL), and the filtrate was evaporated to dryness under reduced pressure. The crude solid product was washed with non-dried MeOH ( $4 \times 3$  mL) to obtain **6** as a dark solid. Yield: 78 mg (85%). Compound **6** fluoresces neither in the solid state nor in solution when irradiated with UV light ( $\lambda_{ex}=366$  nm). Dark gray platelets of **6** suitable for X-ray diffraction were obtained by slow evaporation (Granopent<sup>®</sup>) of a  $CHCl_3$  solution under inert conditions.

$^1H$  NMR (300.0 MHz,  $C_6D_6$ ):  $\delta=1.28$  (s, 36H,  $C(CH_3)_3$ ), 3.38 (s, 12H,  $NMe_2$ ), 6.74 (m, 4H, H-b), 7.62 (dd,  $J=9.2, 2.0$  Hz, 4H, H-3,6), 7.69 (m, 4H, H-a), 8.06 (d,  $J=2.0$  Hz, 4H, H-1,8), 8.64 (d,  $J=9.2$  Hz, 4H, H-4,5);  $^{11}B\{^1H\}$  NMR (96.3 MHz,  $C_6D_6$ ):  $\delta=\sim 75$  ppm ( $h_{1/2}=3500$  Hz);  $^{13}C\{^1H\}$  NMR (75.4 MHz,  $C_6D_6$ ):  $\delta=31.3$  ( $C(CH_3)_3$ ), 34.9 ( $C(CH_3)_3$ ), 45.1 ( $NMe_2$ ), 124.3 (C-3,6), 125.7 (C-4,5), 126.1 (C-1,8), 129.0 (C-4a,10a), 134.0 (C-b), 136.5 (C-8a,9a), 140.1 (C-9), 140.9 (C-a), 145.8 (C-10), 146.5 (C-2,7), 146.6 ppm (C-c); MS (MALDI):  $m/z$  (%): 838 (100) [ $M^+$ ]; elemental analysis calcd (%) for  $C_{60}H_{68}B_2N_2$  (838.78): C 85.91, H 8.17, N 3.34; found: C 86.06, H 8.23, N 3.14.

**4.2.4. Synthesis of 7.** Neat  $nBu_3Sn-C_4H_9S$  (225 mg, 604  $\mu$ mol) was added to a solution of **5** (100 mg, 110  $\mu$ mol) and  $(tBu_3P)_2Pd$  (11 mg, 22  $\mu$ mol) in toluene (5 mL) and the mixture was heated at 80 °C for 48 h. After cooling to rt the solution was evaporated to dryness in vacuo. The crude oily residue was re-dissolved in non-dried  $CHCl_3$  (10 mL) and filtered through a pleated filter paper containing  $MgSO_4$  to remove the catalyst. The filtrate was taken to dryness under reduced pressure and the crude solid product was washed with non-dried MeOH until the extract remained colorless. Compound **7** was obtained as a purple solid and showed a red fluorescence both in solution and in the solid state ( $\lambda_{ex}=366$  nm). Yield: 75 mg (74%).

$^1H$  NMR (300.0 MHz,  $C_6D_6$ ):  $\delta=1.22$  (s, 36H,  $C(CH_3)_3$ ), 6.78 (m, 4H, H-b), 7.13 (dd,  $J=5.1, 3.3$  Hz, 2H, H- $\beta$ ), 7.29 (dd,  $J=5.1, 1.2$  Hz, 2H, H- $\alpha$ ), 7.36 (dd,  $J=3.3, 1.2$  Hz, 2H, H- $\gamma$ ), 7.43 (dd,  $J=9.3, 1.8$  Hz, 4H, H-3,6), 7.67 (m, 4H, H-a), 8.04 (d,  $J=1.8$  Hz, 4H, H-1,8), 8.27 (d,

$J=9.3$  Hz, 4H, H-4,5);  $^{11}B$  NMR (96.3 MHz,  $C_6D_6$ ):  $\delta=n. o.$ ;  $^{13}C\{^1H\}$  NMR (75.4 MHz,  $C_6D_6$ ):  $\delta=31.2$  ( $C(CH_3)_3$ ), 34.8 ( $C(CH_3)_3$ ), 125.2 (C-1,8), 125.4 (C-3,6), 126.9 (C- $\alpha$ ), 127.6 (C- $\beta$ ), 127.6 (C-4,5), 128.4 (C-10), 129.7 (C- $\gamma$ ), 130.5 (C-4a,10a), 134.3 (C-b), 134.9 (C-8a,9a), 140.6 (C- $\delta$ ), 141.0 (C-a), 143.9 (C-9), 146.4 (C-c), 146.8 (C-2,7); MS (MALDI):  $m/z$  (%): 916 (100) [ $M^+$ ]; elemental analysis calcd (%) for  $C_{64}H_{62}B_2S_2$  (916.93): C 83.83, H 6.82, S 6.99; found: C 83.39, H 6.68, S 7.15.

### 4.3. Crystal structure analyses

Compounds **1**, **3**, 9-Cl-2,7-DTBA, 9,10-Br<sub>2</sub>-2,7-DTBA, and **12** were measured on an STOE IPDS-II diffractometer with graphite-monochromated  $MoK\alpha$  radiation ( $\lambda=0.71073$  Å). Equivalent reflections were averaged. An empirical absorption correction with the program PLATON<sup>21</sup> was performed for **1**, **3**, 9-Cl-2,7-DTBA, and 9,10-Br<sub>2</sub>-2,7-DTBA. Compounds **5**, **6**, **7**, and **11** were measured on an STOE IPDS-II diffractometer using a Genix Microfocus X-ray source with mirror optics and  $MoK\alpha$  radiation. The data were corrected for absorption with the frame-scaling procedure contained in the X-AREA package.<sup>22</sup> The structures were solved by direct methods using the program SHELXS<sup>23</sup> and refined with full-matrix least-squares on  $F^2$  using the program SHELXL-97.<sup>24</sup> All H atoms were geometrically positioned and refined using a riding model. The methyl groups bonded to N in compound **6** were allowed to rotate but not to tip.

In compound **5**, one of the co-crystallized toluene molecules is disordered about a center of inversion with equal occupancies; a second toluene molecule is disordered over two positions with a site occupation factor of 0.510(9) for the major occupied site.

In compound **6**, one methyl group of each  $NMe_2$  substituent is disordered over two positions with a site occupation factor of 0.599(17) for the major occupied site.

There are two half molecules and 2.5 molecules of benzene in the asymmetric unit of **7**. Both thiophene rings are disordered over two positions with site occupation factors of 0.504(3) and 0.615(4) for the major occupied sites. The coordinates and displacement parameters of the overlying disordered C and S atoms were constrained to be the same. Two *tert*-butyl groups are disordered over two positions with site occupation factors of 0.673(5) and 0.59(1) for the major occupied sites. The geometric parameters of one of the disordered *tert*-butyl groups were restrained to be equal as those of a not disordered *tert*-butyl group; the disordered atoms of the *tert*-butyl groups were isotropically refined.

Compound **11** crystallizes together with 0.5 equiv of  $C_6H_6$ . One *tert*-butyl group of **11** is disordered over three positions with site occupation factors of 0.330(4), 0.34(1), and 0.33(1). The disordered atoms were isotropically refined and their geometric parameters were restrained to be equal to those of a non-disordered *tert*-butyl group. Both hydroxyl hydrogen atoms were freely refined.

CCDC reference numbers: CCDC-914139 (9,10-Br<sub>2</sub>-2,7-DTBA), 914138 (9-Cl-2,7-DTBA), 914137 (**1**), 914136 (**3**), 914134 (**5**), 914135 (**6**), 930650 (**7**), 930651 (**11**), 930652 (**12**).

### Acknowledgements

M.W. acknowledges financial support by the Beilstein Institute, Frankfurt/Main, Germany, within the research collaboration NanoBiC.

### Supplementary data

Syntheses and characterization of 9,10-Br<sub>2</sub>-2,7-DTBA, 9-Cl-2,7-DTBA, and **1**; details of the X-ray crystal structure analyses of 9,10-Br<sub>2</sub>-2,7-DTBA, 9-Cl-2,7-DTBA, **1**, **11**, and **12**; overlays of the UV/vis absorption spectra of **6**,  $K[6]$ , and  $K_2[6]$ ; cyclic voltammograms of **6** and **7** with different switching potentials; overlays of the UV/vis absorption and fluorescence spectra of **3**, **5**, and **7**;  $^1H$  NMR

spectra of **6** before and after the addition of ethereal HCl; photo-oxidation experiments. Supplementary data associated with this article can be found in the online version, at <http://dx.doi.org/10.1016/j.tet.2013.06.036>.

## References and notes

- (a) *Functional Organic Materials: Syntheses, Strategies and Applications*; Müller, T. J. J., Bunz, U. H. F., Eds.; Wiley-VCH: Weinheim, Germany, 2007; (b) Jäkle, F. *Coord. Chem. Rev.* **2006**, *250*, 1107–1121; (c) Jäkle, F. *Chem. Rev.* **2010**, *110*, 3985–4022.
- (a) Shirakawa, H. *Angew. Chem., Int. Ed.* **2001**, *40*, 2574–2580; (b) MacDiarmid, A. G. *Angew. Chem., Int. Ed.* **2001**, *40*, 2581–2590; (c) Heeger, A. J. *Angew. Chem., Int. Ed.* **2001**, *40*, 2591–2611.
- Müllen, K. *Pure Appl. Chem.* **1993**, *65*, 89–96.
- Müller, U.; Baumgarten, M. *J. Am. Chem. Soc.* **1995**, *117*, 5840–5850.
- Baumgarten, M.; Müller, U.; Bohnen, A.; Müllen, K. *Angew. Chem., Int. Ed. Engl.* **1992**, *31*, 448–451.
- (a) Iwamura, H. *Adv. Phys. Org. Chem.* **1990**, *26*, 179–253; (b) Rajca, A. *Chem. Rev.* **1994**, *94*, 871–893; (c) Ratera, I.; Veciana, J. *Chem. Soc. Rev.* **2012**, *41*, 303–349.
- Fritz, R.; Rettig, W.; Nishiyama, K.; Okada, T.; Müller, U.; Müllen, K. *J. Phys. Chem. A* **1997**, *101*, 2796–2802.
- Rettig, W. *Angew. Chem., Int. Ed. Engl.* **1986**, *25*, 971–988.
- Kang, T. J.; Kahlow, M. A.; Giser, D.; Swallen, S.; Nagarajan, V.; Jarzaba, W.; Barbara, P. F. *J. Phys. Chem.* **1988**, *92*, 6800–6807.
- Kang, T. J.; Jarzaba, W.; Barbara, P. F.; Fonseca, T. *Chem. Phys.* **1990**, *149*, 81–95.
- (a) Hoffend, C.; Schödel, F.; Bolte, M.; Lerner, H.-W.; Wagner, M. *Chem.—Eur. J.* **2012**, *18*, 15394–15405; (b) Hoffend, C.; Diefenbach, M.; Januszewski, E.; Bolte, M.; Lerner, H.-W.; Holthausen, M. C.; Wagner, M. *Dalton Trans.* **2013**, <http://dx.doi.org/10.1039/c3dt51035b>
- Dietrich, M.; Mortensen, J.; Heinze, J. *Angew. Chem., Int. Ed. Engl.* **1985**, *24*, 508–509.
- Cai, J.; Ruffieux, P.; Jaafar, R.; Bieri, M.; Braun, T.; Blankenburg, S.; Muoth, M.; Seitsonen, A. P.; Saleh, M.; Feng, X.; Müllen, K.; Fasel, R. *Nature* **2010**, *466*, 470–473.
- Dou, C.; Saito, S.; Matsuo, K.; Hisaki, I.; Yamaguchi, S. *Angew. Chem., Int. Ed.* **2012**, *51*, 12206–12210.
- (a) Karplus, M.; Pople, J. A. *J. Chem. Phys.* **1963**, *38*, 2803–2807; (b) Günther, H.; Schmickler, H.; Königshofen, H.; Recker, K.; Vogel, E. *Angew. Chem., Int. Ed. Engl.* **1973**, *12*, 243–245; (c) Levin, R. H.; Roberts, J. D. *Tetrahedron Lett.* **1973**, *14*, 135–138; (d) Farnum, D. G. *Adv. Phys. Org. Chem.* **1975**, *11*, 123–175.
- (a) Tickle, I.; Hess, J.; Vos, A.; Engberts, J. B. F. N. *J. Chem. Soc., Perkin Trans. 2* **1978**, 460–465; (b) Adams, H.; Bernad, P. L., Jr.; Eggleston, D. S.; Haltiwanger, R. C.; Harris, K. D. M.; Hembury, G. A.; Hunter, C. A.; Livingstone, D. J.; Kariuki, B. M.; McCabe, J. F. *Chem. Commun.* **2001**, 1500–1501; (c) El-Sayed, M.; Müller, H.; Rheinwald, G.; Lang, H.; Spange, S. *J. Phys. Org. Chem.* **2001**, *14*, 247–255; (d) Aakeröy, C. B.; Beatty, A. M.; Helfrich, B. A.; Nieuwenhuyzen, M. *Cryst. Growth Des.* **2003**, *3*, 159–165.
- Lorbach, A.; Bolte, M.; Lerner, H.-W.; Wagner, M. *Organometallics* **2010**, *29*, 5762–5765.
- (a) Yang, N. C.; Libman, J. *J. Am. Chem. Soc.* **1973**, *95*, 5783–5784; (b) Lishan, D. G.; Hammond, G. S.; Yee, W. A. *J. Phys. Chem.* **1981**, *85*, 3435–3440; (c) Okada, T.; Mataga, N.; Baumann, W.; Siemiarzczuk, A. *J. Phys. Chem.* **1987**, *91*, 4490–4495; (d) Wiessner, A.; Hüttmann, G.; Kühnle, W.; Staerk, H. *J. Phys. Chem.* **1995**, *99*, 14923–14930; (e) Dey, J.; Warner, I. M. *J. Phys. Chem. A* **1997**, *101*, 4872–4878.
- (a) Boden, R. M. *Synthesis* **1975**, 1975, 783–784; (b) Schmidt, R.; Schaffner, K.; Trost, W.; Brauer, H.-D. *J. Phys. Chem.* **1984**, *88*, 956–958; (c) Donkers, R. L.; Workentin, M. S. *J. Am. Chem. Soc.* **2004**, *126*, 1688–1698; (d) Fudickar, W.; Linker, T. *J. Am. Chem. Soc.* **2012**, *134*, 15071–15082; (e) An interesting example of an NHC-stabilized 9-boraanthracene endoperoxide has recently been published: Wood, T. K.; Piers, W. E.; Keay, B. A.; Parvez, M. *Angew. Chem., Int. Ed.* **2009**, *48*, 4009–4012.
- Januszewski, E.; Lorbach, A.; Grewal, R.; Bolte, M.; Bats, J. W.; Lerner, H.-W.; Wagner, M. *Chem.—Eur. J.* **2011**, *17*, 12696–12705.
- Spek, A. L. *J. Appl. Crystallogr.* **2003**, *36*, 7–13.
- Stoe & Cie X-Area; Stoe & Cie: Darmstadt, Germany.
- Sheldrick, G. M. *Acta Crystallogr.* **1990**, *A46*, 467–473.
- Sheldrick, G. M. *SHELXL-97, A Program for the Refinement of Crystal Structures*; Universität Göttingen: Göttingen, Germany.